POLITECNICO
MILANO 1863

DIPARTIMENTO DI MECCANICA

mecc

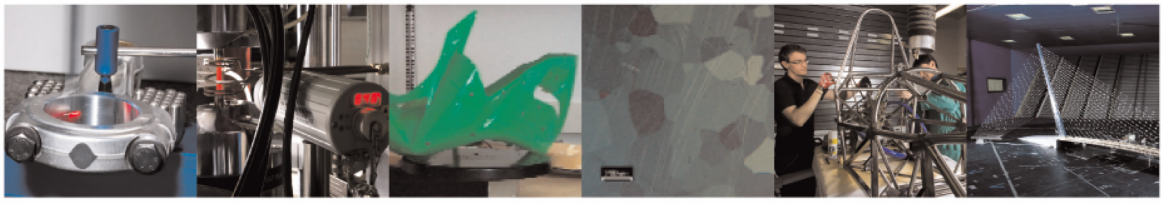

Guidelines for the layout and tuning of piezoelectric resonant shunt with negative capacitances in terms of dynamic compliance, mobility and accelerance

M. Berardengo, S. Manzoni, O. Thomas and M. Vanali

This is a post-peer-review, pre-copyedit version of Berardengo M, Manzoni S, Thomas O, Vanali M. Guidelines for the layout and tuning of piezoelectric resonant shunt with negative capacitances in terms of dynamic compliance, mobility and accelerance. *Journal of Intelligent Material Systems and Structures*. 2021;32(17):2092-2107. The final authenticated version is available online at: http://dx.doi.org/10.1177/1045389X20986991

DIPARTIMENTO DI MECCANICA ■ POLITECNICO DI MILANO
via G. La Masa, 1 ■ 20156 Milano ■ EMAIL (PEC): pecmecc@cert.polimi.it
http://www.mecc.polimi.it
Rev. 0

Journal Title
XX(X):2–25

DOI: ToBeAssigned
www.sagepub.com/

Guidelines for the layout and tuning of piezoelectric resonant shunt with negative capacitances in terms of dynamic compliance, mobility and accelerance

M. Berardengo[1] and S. Manzoni[2] and O. Thomas[3] and M. Vanali[4]

Abstract

This paper addresses the vibration attenuation provided by the resonant piezoelectric shunt enhanced by means of negative capacitances. The shunt impedance is composed by one or two negative capacitances, a resistance and an inductance. It is shown that closed analytical formulations, common to all the possible connections of the negative capacitances, can be derived for the tuning of the circuit components and for the prediction of the attenuation in terms of dynamic compliance, mobility and accelerance. The paper also compares the attenuation performance provided by the two possible layouts for the electrical link between the resistance and the inductance, i.e. series and parallel. Furthermore, this work evidences which shunt configurations offer advantages in terms of practical implementation and the benefits provided by the use of negative capacitances in the shunt circuit. In the last part of the paper, guidelines for the use of resonant shunt are given to the reader and, finally, the theoretical results are validated by means of an experimental campaign showing that it is possible to cancel the resonance on which the resonant shunt is targeted.

Keywords

piezoelectric shunt, resonant shunt, negative capacitance, damping, vibration control

Introduction

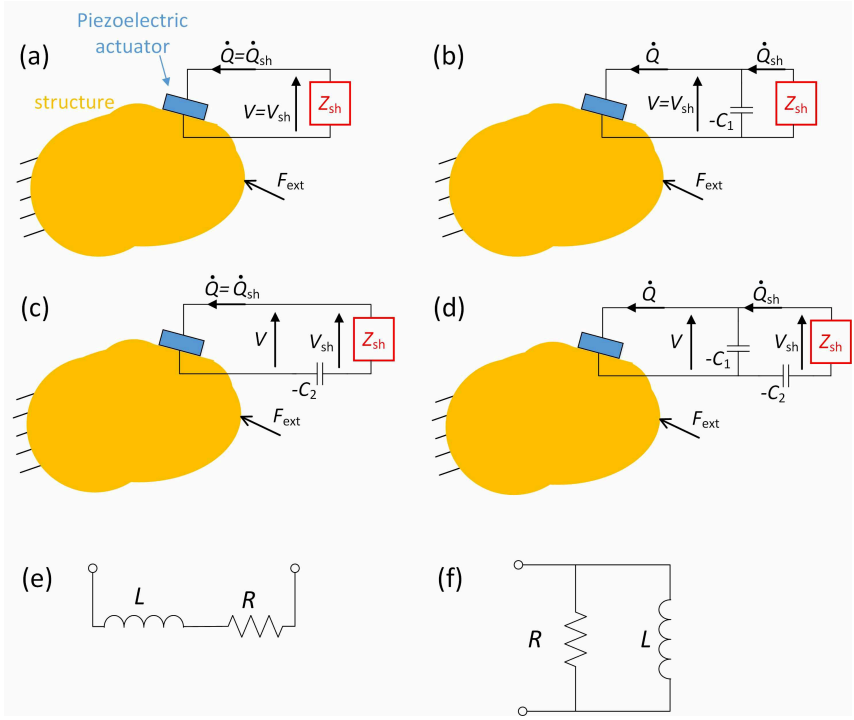

Figure 1. A generic structure with a piezoelectric patch shunted with a passive impedance Z_{sh} (a) and with the addition of NCs in parallel (b), series (c) and SP (d) configuration. Refer to Section 'Model' for the definition of the other symbols in the figure. L and R connected in series (e) and in parallel (f).

[1]Università degli Studi di Genova - Department of Mechanical, Energy, Management and Transportation Engineering - Via Opera Pia, 15A - 16145 Genoa, Italy
[2]Politecnico di Milano - Department of Mechanical Engineering - Via La Masa, 34 - 20156 Milan, Italy
[3]Arts et Métiers Institute of Technology, LISPEN, HESAM Université - 8 bd. Louis XIV 59046 Lille, France
[4]Università degli Studi di Parma - Department of Engineering and Architecture - Parco Area delle Scienze, 181/A - 43124 Parma, Italy

Corresponding author:
Stefano Manzoni
Email: stefano.manzoni@polimi.it

Prepared using sagej.cls

Piezoelectric shunt is a well-known technique for vibration attenuation. The basic principle of the method is the connection between a piezoelectric actuator, which is bonded to a vibrating structure, and a properly designed electrical network (Darleux et al. (2018); Zhao et al. (2015); Gripp and Rade (2018)). The shunt impedance that offers the highest resonance attenuation in case of single-mode control is made from an inductance L and a resistance R (LR-shunt or resonant shunt) connected either in series (Hagood and von Flotow (1991); Berardengo et al. (2016a); Matveenko et al. (2018)) or parallel (Høgsberg and Krenk (2015); Caruso (2001); Gardonio and Casagrande (2017); Andreaus and Porfiri (2007)).

There are two factors able to influence the attenuation performance provided by the piezoelectric shunt: the optimisation of the impedance and the value of the modal electro mechanical coupling factor (MEMCF) k_i of each mode of the electro-mechanical system (which is made from the vibrating structure, the shunt impedance, and the piezoelectric actuator). If an optimally tuned shunt impedance is taken into consideration, then the only way to increase the damping performance is to increase the MEMCF. This parameter depends on the geometrical, electrical and mechanical features of the electro-mechanical system (Thomas et al. (2012, 2009); Ducarne et al. (2012)). It is also possible to prove that the MEMCF of a given mode is function of the distance between the natural frequencies of the electro-mechanical system with the piezoelectric actuator in open- (OC) and short-circuit (SC). An increase/decrease of the MEMCF corresponds to an increase/decrease of the maximum achievable attenuation, as shown in Thomas et al. (2012).

Different works in the literature showed that the attenuation performance provided by passive shunt electric networks can be improved using synthetic circuits (e.g., Date et al. (2000); Beck et al. (2013); Pohl (2017)), and, in particular, the use of Negative Capacitances (NCs), built by employing operational amplifiers, showed to be highly effective and reliable. Indeed, NCs are able to artificially increase the MEMCF and thus to increase the maximum achievable damping performance (Berardengo et al. (2016b, 2017b)). The improved modal electro mechanical coupling factor will be referred here as enhanced modal electro mechanical coupling factor (EMEMCF) $\tilde{k}_i$. NCs have fruitfully been coupled to different passive shunt impedances. Particularly, the coupling with the resonant shunt (de Marneffe and Preumont (2008); Neubauer et al. (2006)) showed high performances for single-mode vibration attenuation, keeping a simple layout.

This shunt network admits several configurations as function of the connection between the piezoelectric actuator and the NCs and between the resistance and the inductance. Indeed, the piezoelectric actuator can be connected to a passive shunt impedance Z_{sh}, made from a resistance R and an inductance L (linked in either parallel or series), and the NCs in three different ways: parallel, series and series+parallel (SP) (Berardengo et al. (2016b, 2017b, 2015)), as explained in Figs. 1a-d ($-C_1$ indicates the NC in parallel configuration, while $-C_2$ indicates the NC connected in series). Moreover, the control target can change as a function of the application (i.e. displacement, velocity, acceleration). Even if most of the articles related to the piezoelectric shunt damping focus on the vibration reduction in terms of displacement, it is highly likely to face situations where the control target must be different. As an example, if the vibration reduction is

aimed at lowering sound emission, velocity must be reduced due to the relation between surface velocity and the consequent emitted noise (Bricault et al. (2019)). In other cases, where inertial actions must be reduced, the vibration control must be optimised in terms of acceleration (e.g. Zhu et al. (2020)).

In this article, general analytical formulations are proposed for the optimisation of the resonant shunt when coupled to NCs referring to various target variables (i.e. displacement, velocity and acceleration) and the possible layouts for the connection of L and R (series or parallel). This work is thus intended as an extension of (Berardengo et al. (2018)), where the optimisation is carried out only in terms of displacement. The aim of the proposed study is to provide the user with guidelines for the choice of the best layout and tuning of resonant shunt for the given problem and to suggest solution to overcome the most critical feasibility issues. This was made possible by the new outcomes of the proposed analyses. Indeed, the manuscript:

- provides formulations for the tuning of the shunt impedance when velocity and acceleration are the control variables. This constitutes a generalisation of the formulations presented in (Berardengo et al. (2018)) for attenuating displacement. Furthermore, formulations for the prediction of the attenuation are presented;
- evidences that, when NCs are added in the shunt, the optimal values of L and R for displacement, velocity and acceleration become increasingly different when the NC effects increase. This implies the importance of using the proper tuning formulation, especially when NCs are used;
- shows which connection between L and R (i.e. either series or parallel) is convenient when NCs are used, not just considering the attenuation performance, but also taking into account implementation problems. It will be shown that the series connection allows to have lower values for the inductance, implying an easier practical implementation, especially when the NC effects increase. Moreover, the series connection when NCs are used in the shunt shows the same level of robustness to mistuning compared to the parallel connection, in contrast to what occurs when NCs are not employed (see Yamada et al. (2010));
- proposes a method for lowering the value of the shunt inductance without deteriorating the attenuation performance. The proposed approach allows to decrease the complexity of the practical implementation of the shunt circuit and, at the same time, enables to improve the vibration attenuation;
- presents a sensitivity analysis with respect to the presence of modes different than that under control. The analytical procedures in the literature (and in this work) applied to derive the optimal values of L and R (either with or without NCs) are usually based on single-degree-of-freedom models. However, there are few studies in the literature that outline the influence of the other modes on the attenuation provided by the calculated optimal L and R values. This paper presents some analyses to show the effect of modes close to that under control and to discuss the reliability of the optimal values derived for L and R with a single-degree-of-freedom approach.

Table 1. Definition of $C_{\rm eq}$ without NCs, enhanced by a single NC in either parallel or series configuration, and enhanced by two NCs for the SP configuration

	simple shunt without NCs	Parallel config.	Series config.	SP config.
$C_{\rm eq}$ =	$C_{{\rm p}i}$	$(C_{{\rm p}i}-C_1)$	$\frac{C_{{\rm p}i}C_2}{C_2-C_{{\rm p}i}}$	$\frac{(C_{{\rm p}i}-C_1)C_2}{C_1+C_2-C_{{\rm p}i}}$

Table 2. Expressions of A, B, C and D for the different possible cases (see Eq. (4)). Here, $E=\xi_i\omega_i(\omega_{\rm e}^2-\Omega^2)$ and $G=\Omega^2(\omega_{\rm e}^2+4\xi_i\xi_{\rm e}\omega_i\omega_{\rm e}+(\omega_i^{\rm oc})^2)$

	L and R connected in parallel	L and R connected in series
dynamic compliance	$A_{\rm p}^{\rm disp}$=$\omega_{\rm e}^2-\Omega^2$	$A_{\rm s}^{\rm disp}$=$A_{\rm p}^{\rm disp}$
	$B_{\rm p}^{\rm disp}$=$2\xi_{\rm e}\omega_{\rm e}\Omega$	$B_{\rm s}^{\rm disp}$=$B_{\rm p}^{\rm disp}$
	$C_{\rm p}^{\rm disp}$=$\Omega^4-G+(\omega_i^{\rm sc})^2\omega_{\rm e}^2$	$C_{\rm s}^{\rm disp}=C_{\rm p}^{\rm disp}$
	$D_{\rm p}^{\rm disp}$=$2\Omega[\xi_{\rm e}\omega_{\rm e}((\omega_i^{\rm sc})^2-\Omega^2)+E]$	$D_{\rm s}^{\rm disp}$=$2\Omega[\xi_{\rm e}\omega_{\rm e}((\omega_i^{\rm oc})^2-\Omega^2)+E]$
mobility	$A_{\rm p}^{\rm vel}$=$-\Omega B_{\rm p}^{\rm disp}$	$A_{\rm s}^{\rm vel}$=$-\Omega B_{\rm s}^{\rm disp}$
	$B_{\rm p}^{\rm vel}$=$\Omega A_{\rm p}^{\rm disp}$	$B_{\rm s}^{\rm vel}$=$\Omega A_{\rm s}^{\rm disp}$
	$C_{\rm p}^{\rm vel}$=$C_{\rm p}^{\rm disp}$	$C_{\rm s}^{\rm vel}$=$C_{\rm s}^{\rm disp}$
	$D_{\rm p}^{\rm vel}$=$D_{\rm p}^{\rm disp}$	$D_{\rm s}^{\rm vel}$=$D_{\rm s}^{\rm disp}$
accelerance	$A_{\rm p}^{\rm acc}$=$-\Omega^2 A_{\rm p}^{\rm disp}$	$A_{\rm s}^{\rm acc}$=$-\Omega^2 A_{\rm s}^{\rm disp}$
	$B_{\rm p}^{\rm acc}$=$-\Omega^2 B_{\rm p}^{\rm disp}$	$B_{\rm s}^{\rm acc}$=$-\Omega^2 B_{\rm s}^{\rm disp}$
	$C_{\rm p}^{\rm acc}$=$C_{\rm p}^{\rm disp}$	$C_{\rm s}^{\rm acc}$=$C_{\rm s}^{\rm disp}$
	$D_{\rm p}^{\rm acc}$=$D_{\rm p}^{\rm disp}$	$D_{\rm s}^{\rm acc}$=$D_{\rm s}^{\rm disp}$

Model

The model used in this paper was originally developed in Thomas et al. (2012, 2009) and Ducarne et al. (2012). Then, Berardengo et al. (2016b, 2017b) enhanced its accuracy, thanks to an improved description of the electrical behaviour of the system and, in particular, defining the capacitance value of the piezoelectric patch $C_{\rm pi}$, when a single-degree-of-freedom approximation of the system is considered, which takes into account the contribution of the modes higher than the i-th ($C_{\rm pi}$ can be roughly seen as the value of the capacitance of the piezoelectric actuator at a frequency value between the i-th and the $(i+1)$-th modes). Here, the model is briefly recalled for the sake of clarity.

A generic elastic structure excited by an external force $F_{\rm ext}$ is taken into account (Figs. 1a-d). One piezoelectric patch is bonded to this structure and a generic passive impedance $Z_{\rm sh}$ is shunted to the piezoelectric patch. The symbol V in Figs. 1a-d indicates the voltage between the electrodes of the piezoelectric actuator, while the symbol Q is used to indicate the electric charge in one of the electrodes. $V_{\rm sh}$ and $Q_{\rm sh}$ in Figs. 1a-d

Table 3. Definition of the parameters ω_e and ξ_e for the two connection types of R and L

	L and R connected in series	L and R connected in parallel
$\omega_e =$	$\sqrt{\frac{1}{LC_{eq}}}$	$\sqrt{\frac{1}{LC_{eq}}}$
$\xi_e =$	$\frac{R}{2}\sqrt{\frac{C_{eq}}{L}}$	$\frac{1}{2R}\sqrt{\frac{L}{C_{eq}}}$

are the voltage and the charge seen by the shunt impedance Z_{sh}, respectively, and they coincide with V and Q when no NCs are connected to the actuator (Fig. 1a).

The displacement $U(x,t)$ of any point x of the structure at time t can be expressed as a function of the modal coordinates q_i and the eigenmodes Φ_i of the system calculated with the piezoelectric patch in SC and scaled to the unit modal mass, where $i = 1, ..., N$, being N the number of vibration eigenmodes.

Considering the case of low modal density, it is possible to describe the electro-mechanical system dynamics by means of a single-degree-of-freedom approximation. The system dynamics can be thus modelled, for Ω close to ω_i (Ω indicates the angular frequency and ω_i the i-th natural frequency of the electro-mechanical system in SC), by writing the following equations:

$$\ddot{q}_i + 2\xi_i\omega_i\dot{q}_i + (\omega_i^{sc})^2 q_i - \omega_i\tilde{k}_i\bar{V}_{sh} = F_i \tag{1}$$

$$\bar{V}_{sh} - \bar{Q}_{sh} + \omega_i\tilde{k}_i q_i = 0 \tag{2}$$

where F_i is the modal forcing, ξ_i is the non-dimensional damping ratio associated to the i-th mode, $\bar{V}_{sh} = V_{sh}\sqrt{C_{eq}}$ and $\bar{Q}_{sh} = Q_{sh}/\sqrt{C_{eq}}$. The variable C_{eq} is an equivalent capacitance whose value depends of the NC values (see Tab. 1). The symbol ω_i^{sc} indicates the i-th natural frequency of the electro-mechanical system when Z_{sh} is an SC ($V_{sh} = 0$). Similarly, it is possible to define ω_i^{oc} as the i-th natural frequency of the electro-mechanical system when Z_{sh} is an OC ($Q_{sh} = 0$). The values of ω_i^{oc} and ω_i^{sc} change depending on whether an NC is connected to the piezoelectric actuator or not, and on its layout (Figs. 1a-d). The analytical expressions of ω_i^{oc} and ω_i^{sc} can be found in (Berardengo et al. (2016b)).

Equation (1) describes the motion of the electro-mechanical system, while Eq. (2) describes the dynamics of the electrical part of the system.

The main effect of the NCs in the shunt circuit is to artificially increase the value of the MEMCF k_i and thus to improve the control performances (Berardengo et al. (2016b)).

Particularly, the effect of an NC in parallel connection is to shift the OC eigenfrequencies towards higher frequency values, while the effect of an NC in series is to shift the SC eigenfrequencies towards lower frequency values; the SP configuration, instead, both decreases the SC and increases the OC eigenfrequencies at the same time. In light of this, the use of NCs always leads to an increase of the distance between the SC and OC eigenfrequencies and thus to an increase of k_i. Therefore, it is possible to define the new parameter $\tilde{k}_i$ (the EMEMCF). Under the hypothesis of low modal density, this new parameter can be accurately approximated as:

$$|\tilde{k}_i| \simeq \sqrt{\frac{(\omega_i^{\mathrm{oc}})^2 - (\omega_i^{\mathrm{sc}})^2}{\omega_i^2}} \tag{3}$$

It is noticed that $|\tilde{k}_i| = |k_i|$ when no NCs are used, otherwise $|\tilde{k}_i| > |k_i|$ (Berardengo et al. (2016b)). Since k_i is related to the energy transfer between the i-th mode and the electric circuit and vice versa (Thomas et al. (2012)), it is possible to conclude that $\tilde{k}_i$ represents the improvement in the energy transfer guaranteed by the use of NCs in the circuit because of the analogy between k_i and $\tilde{k}_i$.

If the generic passive impedance Z_{sh} is composed by an inductance L and a resistance R, the traditional resonant shunt coupled to NCs is obtained (RL-NC shunt). L and R can be connected in either series or parallel (Figs. 1e and f, respectively). Thus, there are six possible configurations for the RL-NC shunt (i.e. two possible layouts for the link between L and R and three different NC configurations).

From Eqs. (1) and (2), it is possible to derive the analytical expressions of the frequency response function (FRF) between F_i and the modal displacement q_i for R and L in parallel ($H_{i,\mathrm{p}}^{\mathrm{disp}}(\mathrm{j}\Omega)$) and in series ($H_{i,\mathrm{s}}^{\mathrm{disp}}(\mathrm{j}\Omega)$) (where j is the imaginary unit). These two FRFs are valid for all the NC types, and also when no NCs are used if the appropriate electro-mechanical system parameter values are employed.

The corresponding FRFs in terms of modal velocity $\dot{q}_i$ over modal force F_i (mobility, superscript 'vel') can be obtained by multiplying $H_i^{\mathrm{disp}}(\mathrm{j}\Omega)$ by $\mathrm{j}\Omega$, while the FRFs in terms of modal acceleration $\ddot{q}_i$ over modal force F_i (accelerance, superscript 'acc') can be achieved by multiplying $H_i^{\mathrm{disp}}(\mathrm{j}\Omega)$ by $(-\Omega^2)$.

All the FRFs can be generically expressed as:

$$H_i(\mathrm{j}\Omega) = \frac{A + \mathrm{j}B}{C + \mathrm{j}D} \tag{4}$$

where the coefficients A, B, C and D for the different possible cases are defined in Tab. 2. The above FRFs are expressed as functions of ξ_{e} and ω_{e} which are the non-dimensional damping ratio and the resonant frequency of the electrical circuit, respectively. The analytical expressions of these two parameters are provided in Tab. 3 for both the types of connection between L and R.

Since the NCs are active elements, it is important to recall that the stability of the electro-mechanical system must be checked. The stability conditions are provided in (Berardengo et al. (2018)), and they depend upon the relationships between the values

Table 4. Expressions of $\omega_{\mathrm{e}}^{\mathrm{opt}}$ and $\xi_{\mathrm{e}}^{\mathrm{opt}}$ for the different possible cases. Here $T = 14(\omega_i^{\mathrm{oc}})^2(\omega_i^{\mathrm{sc}})^2$.

	L and R connected in parallel	L and R connected in series
dynamic compliance	$\omega_{\mathrm{e}}^{\mathrm{opt}} = \sqrt{\frac{3(\omega_i^{\mathrm{sc}})^2-(\omega_i^{\mathrm{oc}})^2}{2}}$ $\xi_{\mathrm{e}}^{\mathrm{opt}} = \frac{\sqrt{3}}{2}\sqrt{\frac{(\omega_i^{\mathrm{oc}})^2-(\omega_i^{\mathrm{sc}})^2}{3(\omega_i^{\mathrm{sc}})^2-(\omega_i^{\mathrm{oc}})^2}}$	$\omega_{\mathrm{e}}^{\mathrm{opt}} = \omega_i^{\mathrm{oc}}$ $\xi_{\mathrm{e}}^{\mathrm{opt}} = \frac{\sqrt{3}}{2}\sqrt{\frac{(\omega_i^{\mathrm{oc}})^2-(\omega_i^{\mathrm{sc}})^2}{(\omega_i^{\mathrm{oc}})^2+(\omega_i^{\mathrm{sc}})^2}}$
mobility	$\omega_{\mathrm{e}}^{\mathrm{opt}} = \omega_i^{\mathrm{sc}}$ $\xi_{\mathrm{e}}^{\mathrm{opt}} = \frac{\sqrt{3}}{2\sqrt{2}}\sqrt{\frac{(\omega_i^{\mathrm{oc}})^2}{(\omega_i^{\mathrm{sc}})^2}-1}$	$\omega_{\mathrm{e}}^{\mathrm{opt}} = \frac{\sqrt{2}(\omega_i^{\mathrm{oc}})^2}{\sqrt{(\omega_i^{\mathrm{oc}})^2+(\omega_i^{\mathrm{sc}})^2}}$ $\xi_{\mathrm{e}}^{\mathrm{opt}} = \frac{\sqrt{[(\omega_i^{\mathrm{oc}})^2-(\omega_i^{\mathrm{sc}})^2][5(\omega_i^{\mathrm{oc}})^4+T+5(\omega_i^{\mathrm{sc}})^4]}}{4\omega_i^{\mathrm{oc}}[(\omega_i^{\mathrm{oc}})^2+(\omega_i^{\mathrm{sc}})^2]}$
accelerance	$\omega_{\mathrm{e}}^{\mathrm{opt}} = \sqrt{\frac{(\omega_i^{\mathrm{oc}})^2+(\omega_i^{\mathrm{sc}})^2}{2}}$ $\xi_{\mathrm{e}}^{\mathrm{opt}} = \frac{\sqrt{3}}{2\sqrt{2}}\sqrt{\frac{(\omega_i^{\mathrm{oc}})^2}{(\omega_i^{\mathrm{sc}})^2}-1}$	$\omega_{\mathrm{e}}^{\mathrm{opt}} = \frac{(\omega_i^{\mathrm{oc}})^2}{\omega_i^{\mathrm{sc}}}$ $\xi_{\mathrm{e}}^{\mathrm{opt}} = \frac{\sqrt{3}}{2\sqrt{2}}\sqrt{1-\frac{(\omega_i^{\mathrm{sc}})^2}{(\omega_i^{\mathrm{oc}})^2}}$

of the NCs and the value of the blocked piezoelectric capacitance C_∞ and that of the piezoeletric capacitance at the null frequency C_0.

Shunt impedance optimisation

The first element of the shunt impedance to be optimised is the NC. Different works in the literature (e.g. Berardengo et al. (2016b)) explain that the closer the NCs are to the value of $C_{\mathrm{p}i}$ (always respecting the stability limits), the higher $\tilde{k}_i$ is and thus the higher the maximum achievable attenuation is.

The other elements to be optimised are L and R.

Optimisation of the value of the inductance

The optimisation of the value of L (as well as that of R) is carried out in this paper by using a commonly-accepted procedure which was previously applied to tuned mass dampers and simple piezoelectric resonant shunts without NCs (e.g., Hagood and von Flotow (1991); Thomas et al. (2012)). Basically, it is aimed at minimising the maximum of the FRF amplitude of the electro-mechanical system in correspondence of a given mode. It is also noticed that when the control target is displacement, the maximum of the amplitude of the FRF q_i/F_i is taken into consideration; when the target is velocity, the FRF considered is $\dot{q}_i/F_i$, and, finally, when the target is acceleration, the FRF used is $\ddot{q}_i/F_i$.

Furthermore, it is noticed that, since single mode control is taken into account, there is just a multiplicative constant (that is a function of Φ_i) between modal and point FRFs. Therefore, the values of the tuning parameters used for the attenuation in terms of modal displacement are also the optimal values for attenuating point displacement. The same applies to velocity and acceleration.

The method used to derive the optimal inductance is briefly summarised, and it is based on considerations on the shape of the electro-mechanical system FRF. At first, the procedure optimises the value of the electrical frequency ω_e. If an electro-mechanical system with null damping (i.e. $\xi_i = 0$) is considered, there exist two points F^- and F^+ at $\omega_{\mathrm{F}-}$ and $\omega_{\mathrm{F}+}$, respectively, where all the curves $|H_i(\Omega)|$ cross, for a given value of ω_e when ξ_e is varied (refer to (Thomas et al. (2012); Berardengo et al. (2018)) for more details). The value of ω_e considered as optimal (indicated as $\omega_\mathrm{e}^\mathrm{opt}$) is such that $|H_i(\Omega = \omega_{\mathrm{F}-})| = |H_i(\Omega = \omega_{\mathrm{F}+})|$.

The expressions of $\omega_\mathrm{e}^\mathrm{opt}$ for the different possible cases are provided in Tab. 4. Moreover, the expressions of $\omega_{\mathrm{F}-}^2$ and $\omega_{\mathrm{F}+}^2$ for L and R in parallel (valid in case of dynamic compliance, mobility and accelerance) are:

$$\frac{2\omega_\mathrm{e}^2 + (\omega_i^\mathrm{oc})^2 + (\omega_i^\mathrm{sc})^2 \pm \sqrt{[2\omega_\mathrm{e}^2 + (\omega_i^\mathrm{oc})^2 + (\omega_i^\mathrm{sc})^2]^2 - 16\omega_\mathrm{e}^2(\omega_i^\mathrm{sc})^2}}{4} \tag{5}$$

The expressions for L and R in series are:

$$\frac{\omega_\mathrm{e}^2 + (\omega_i^\mathrm{oc})^2 \pm \sqrt{(\omega_i^\mathrm{oc})^4 + \omega_\mathrm{e}^2[\omega_\mathrm{e}^2 - 2(\omega_i^\mathrm{sc})^2]}}{2} \tag{6}$$

The proper expression of $\omega_\mathrm{e}^\mathrm{opt}$ (Tab. 4) must be used to find $\omega_{\mathrm{F}-}$ and $\omega_{\mathrm{F}+}$ in optimal tuning condition for each considered case.

Finally, the corresponding value of L^opt (i.e. the optimal value of the inductance) can be found using the expressions in Tab. 3.

Optimisation of the value of the resistance

After the tuning of ω_e, the optimisation is carried out on the electrical damping ξ_e (again under the hypothesis of ξ_i=0).

The optimal value of ξ_e would be such that both the points F^- and F^+ are maxima of $|H_i(\Omega)|$. However, Thomas et al. (Thomas et al. (2012)) explained that this is not possible. Anyway, two values of ξ_e (here indicated as ξ_e^- and ξ_e^+) exist such that either F^- or F^+ is a maximum of the FRF amplitude, respectively. The optimal value of ξ_e (indicated here as $\xi_\mathrm{e}^\mathrm{opt}$) is set as the geometric mean of ξ_e^+ and ξ_e^-: $(\xi_\mathrm{e}^\mathrm{opt})^2 = [(\xi_\mathrm{e}^+)^2 + (\xi_\mathrm{e}^-)^2]/2$. The expression of $\xi_\mathrm{e}^\mathrm{opt}$ for the different possible cases is provided in Tab. 4.

Finally, the corresponding value of R^opt (i.e. the optimal value of the resistance) can be derived using the expressions presented in Tab. 3. The FRF amplitude with $\xi_\mathrm{e}^\mathrm{opt}$ and $\omega_\mathrm{e}^\mathrm{opt}$ can be seen in Fig. 2 for the dynamic compliance, the mobility and the accelerance (see the red thin solid line in plot (a), the blue thin dashed line in plot (b) and the orange thick solid line in plot (c), respectively).

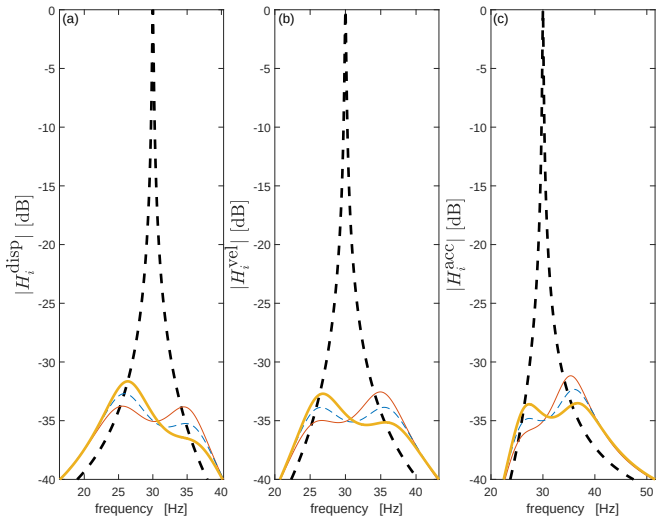

Figure 2. FRFs for a system with k_i=0.3, $\tilde{k}_i$=0.4, ξ_i=0.3%, $\omega_i/(2\pi)$ =30 Hz, NC connected in series, and L and R connected in series. FRFs in terms of dynamic compliance (i.e. $|H_i|^{\mathrm{disp}}$) (a), FRFs in terms of mobility (i.e. $|H_i|^{\mathrm{vel}}$) (b), and FRFs in terms of accelerance (i.e. $|H_i|^{\mathrm{acc}}$) (c). Thick dashed line for FRFs with the piezoelectric patch in SC (without NCs), thin solid line for FRFs with L and R set using the criteria found for the dynamic compliance optimisation, thin dashed line for FRFs with L and R set using the criteria found for the mobility optimisation, and thick solid line for FRFs with L and R set using the criteria found for the accelerance optimisation.

A remarkable result of Tab. 4 and Eqs. 5 and 6 is that the obtained optimisation formulas are general and common to all the possible NC layouts (i.e. SP, series, parallel). This is possible because $\omega_{\mathrm{e}}^{\mathrm{opt}}$, ω_{F^-}, ω_{F^+}, and $\xi_{\mathrm{e}}^{\mathrm{opt}}$ are expressed as functions of ω_i^{oc} and ω_i^{sc}, which depend on the NC layout, as mentioned. Furthermore, these expressions are common also to the case of a pure resonant shunt without the addition of NCs. As a proof of this, it can be also noticed that the expressions gathered in Tab. 4 and Eqs. 5 and 6, in the case of absence of NCs in the shunt circuit, equal the formulations for the simple resonant shunt without the addition of NCs proposed in Thomas et al. (2012) and Yamada et al. (2010).

Controlled FRFs

The optimisation formulas of Tab. 4 are used here to illustrate an example of the achievable results. Figure 2 shows the FRFs for a system chosen as example. Plot (a) shows the FRFs in terms of dynamic compliance, plot (b) depicts the FRFs in terms of mobility, and plot (c) shows the FRFs in terms of accelerance.

This figure evidences that the attenuation levels achieved for the dynamic compliance, mobility, and accelerance FRFs (using the corresponding optimisation criterion) are close each other (as will be shown in more detail further in the paper) (differences lower than 1

dB in Fig. 2 and up to few decibels in case of higher $\tilde{k}_i$ values). Of course, it is important to employ the correct criterion, according to the desired type of optimisation, because the three different optimisation criteria lead to different results (i.e. compare the three controlled FRFs in each plot of Fig. 2).

It is noticed that, when the hypothesis of low modal density is not satisfied, the optimal values of L and R can be slightly different from those obtained from the optimal formulations of Tab. 4 because of the influence of the other modes (Høgsberg and Krenk (2017); Toftekær et al. (2018)) (indeed, the optimisation criteria are based on considerations about the single-degree-of-freedom FRF shape and, if the contribution of the other modes is not negligible, the FRF shape changes). However, even when the hypothesis of low modal density is not satisfied, the expressions reported in Tab. 4 can be still considered as the reference values of $\omega_{\mathrm{e}}^{\mathrm{opt}}$ and $\xi_{\mathrm{e}}^{\mathrm{opt}}$ from which the perfect tuning has to be looked for. A further discussion related to the case of high modal density is provided further in the paper.

Trends of the tuning parameters

This subsection focuses on the differences in terms of values of $\omega_{\mathrm{e}}^{\mathrm{opt}}$ and $\xi_{\mathrm{e}}^{\mathrm{opt}}$ between the two connection types of L and R (i.e. series and parallel), when NCs are used in the shunt circuit, and among the different control variables (i.e. displacement, velocity and acceleration). Since NCs in series are effective for controlling modes at low frequency, while NCs in parallel are effective for controlling modes at high frequency (Berardengo et al. (2016b, 2018)), these two layouts are not compared here because they are usually used for different control problems. In this analysis, the case of NCs in SP configuration is not explicitly treated because its results are not far from those related to the case of the NC in series (Berardengo et al. (2018)).

Figure 3 shows the trends of $\omega_{\mathrm{e}}^{\mathrm{opt}}$ (normalised over the value of ω_i) and $\xi_{\mathrm{e}}^{\mathrm{opt}}$ for a system with k_i=0.1 and an NC in either parallel or series. If the value of k_i is changed, the trends remain close to those of the figure and thus just a single case is shown here for the sake of conciseness.

It is evident that, when $\tilde{k}_i$ increases thanks to the use of the NC, the values of $\omega_{\mathrm{e}}^{\mathrm{opt}}$ for the different optimisations (i.e. displacement, velocity and acceleration) become farther and farther. The same applies to the values of $\xi_{\mathrm{e}}^{\mathrm{opt}}$. This means that it is more and more important to use the proper optimisation criteria, according to the type of variable to be attenuated, when $\tilde{k}_i$ increases. The only exception is related to the values of $\xi_{\mathrm{e}}^{\mathrm{opt}}$ for acceleration and velocity: they are equal in case of parallel connection of L and R (see Tab. 4), while they are different but really close in case of series connection.

Another point is worthy of attention. Analysing the trends of $\omega_{\mathrm{e}}^{\mathrm{opt}}$ (Figs. 3a and c), one can notice that the trends for series and parallel connections of L and R diverge when $\tilde{k}_i$ increases. Due to the definition of $\omega_{\mathrm{e}}^{\mathrm{opt}}$ in Tab. 3, this directly implies that also the resulting values of L^{opt} for the two types of connection will diverge increasing $\tilde{k}_i$. As shown in Figs. 4a and c, the series connection of L and R always allows to have values of L^{opt} lower than those related to the parallel connection. This translates in an easier practical implementation of the shunt circuit. Moreover, when an NC in series is

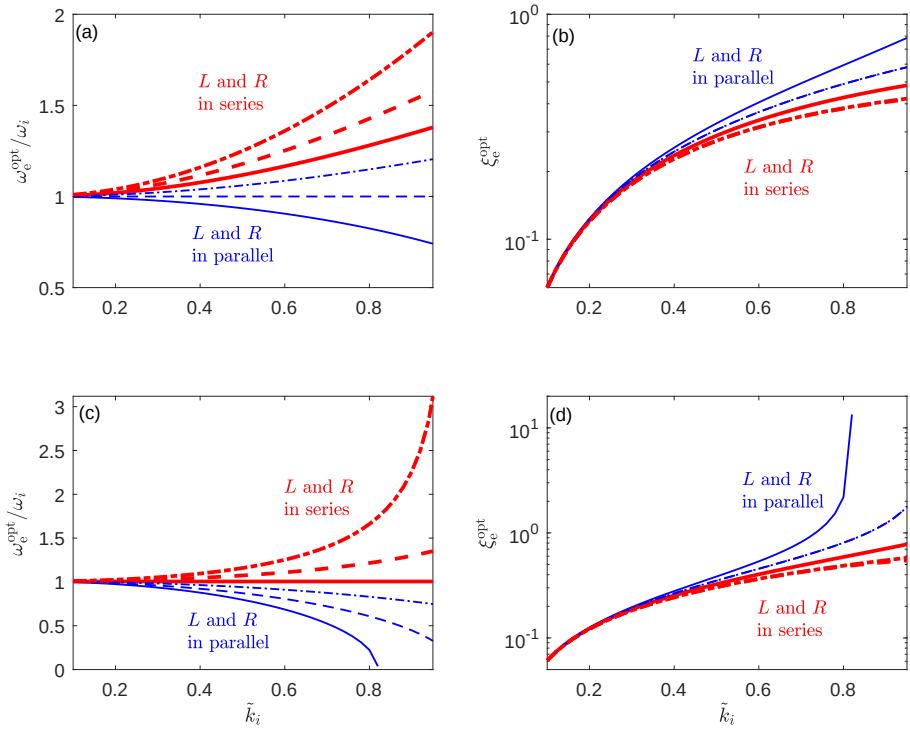

Figure 3. Trends of ω_e^{opt} (normalised over ω_i) and ξ_e^{opt} as a function of $\tilde{k}_i$ for a system with k_i=0.1: NC in parallel for plots (a) and (b), and NC in series for plots (c) and (d). Red thick lines for R and L connected in series and blue thin lines for R and L connected in parallel. Solid line for control in displacement, dashed line for velocity and dash-dotted line for acceleration.

used together with L and R connected in series, a strong decrease of the value of L^{opt} occurs increasing $\tilde{k}_i$ (see Fig. 4c). This is due to two different factors: when a series NC is used, the value of ω_e^{opt} (see Fig. 3c) and the value of C_{eq} (see Tab. 1) increase when $\tilde{k}_i$ increases (i.e. when the value of C_2 becomes closer and closer to C_{pi}). Both these effects lead to a decrease of the value of L^{opt} (see Tab. 3).

Even if many works in the literature (e.g. Fleming et al. (2003)) suggest to add a positive capacitance in parallel to the piezoelectric actuator to decrease the high value of L^{opt} that is encountered when controlling modes at low frequency, here it is evident that an alternative approach is to add an NC in series. This latter solution has the advantage to improve the attenuation performance, while the former deteriorates the vibration attenuation. Therefore, this analysis evidences a new and advantageous approach for solving the problem of high L^{opt} values in resonant shunt.

Considering the trends of ξ_e^{opt} (see Figs. 3b and d), a divergence of the trends for the two different types of connection of L and R is found. However, due to the different

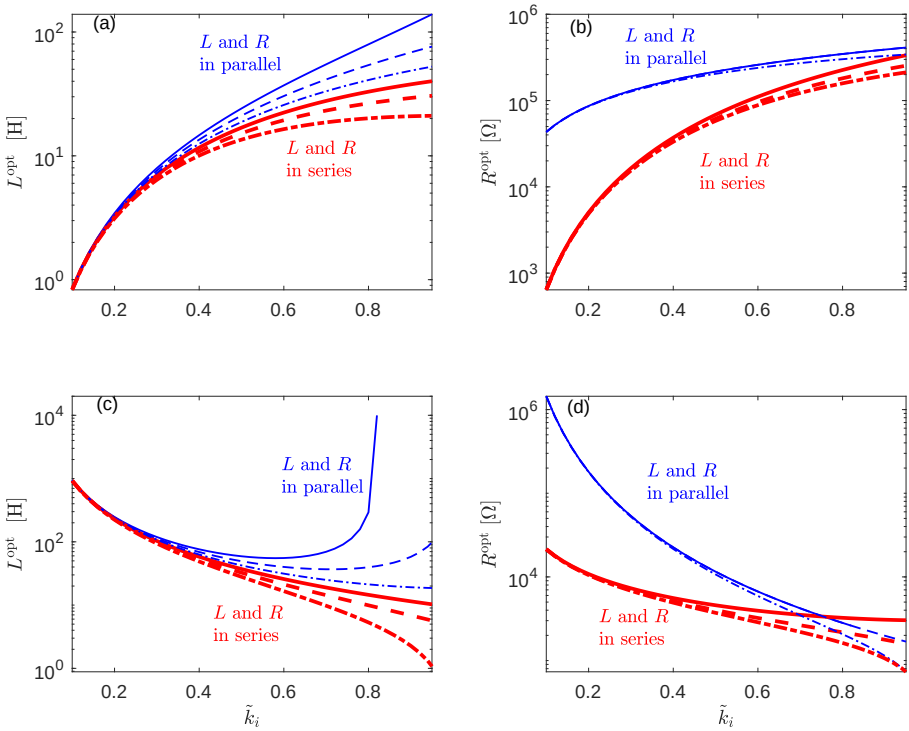

Figure 4. Trends of $L^{\rm opt}$ and $R^{\rm opt}$ as a function of $\tilde{k}_i$ for a system with k_i=0.1: NC in parallel with $\omega_i/(2\pi)$=1000 Hz for plots (a) and (b), and NC in series with $\omega_i/(2\pi)$=30 Hz for plots (c) and (d). Red thick lines for R and L connected in series and blue thin lines for R and L connected in parallel. Solid line for control in displacement, dashed line for velocity and dash-dotted line for acceleration.

definitions of the electric damping (see Tab. 3), this implies that the values of $R^{\rm opt}$ tend to become closer and closer when $\tilde{k}_i$ increases (see Figs. 4b and d). Yamada et al. evidenced in (Yamada et al. (2010)) that the connection of R and L in parallel is advantageous in terms of robustness to possible mistuning for low values of k_i because of the higher values of $R^{\rm opt}$. However, the use of NCs tends to make this advantage of lower and lower importance because the values of $R^{\rm opt}$ become closer and closer increasing the value of $\tilde{k}_i$ (or, in some cases, $R^{\rm opt}$ becomes even higher for L and R connected in series, see Fig. 4d).

A final point to be evidenced is related to the case of an NC connected in series and L and R linked in parallel (see Figs. 3c and d and Figs. 4c and d). In this case the curves related to the control in terms of displacement stop for $\tilde{k}_i \simeq 0.8$. This is because the formulas for the optima cannot be used for such high values of $\tilde{k}_i$ because the quantity $[3(\omega_i^{\rm sc})^2 - (\omega_i^{\rm oc})^2]$ in the expressions of $\omega_{\rm e}^{\rm opt}$ and $\xi_{\rm e}^{\rm opt}$ becomes negative, thus making

them imaginary (see Tab. 4). This problem does not occur for the optimisation in terms of either velocity or acceleration.

Attenuation performance

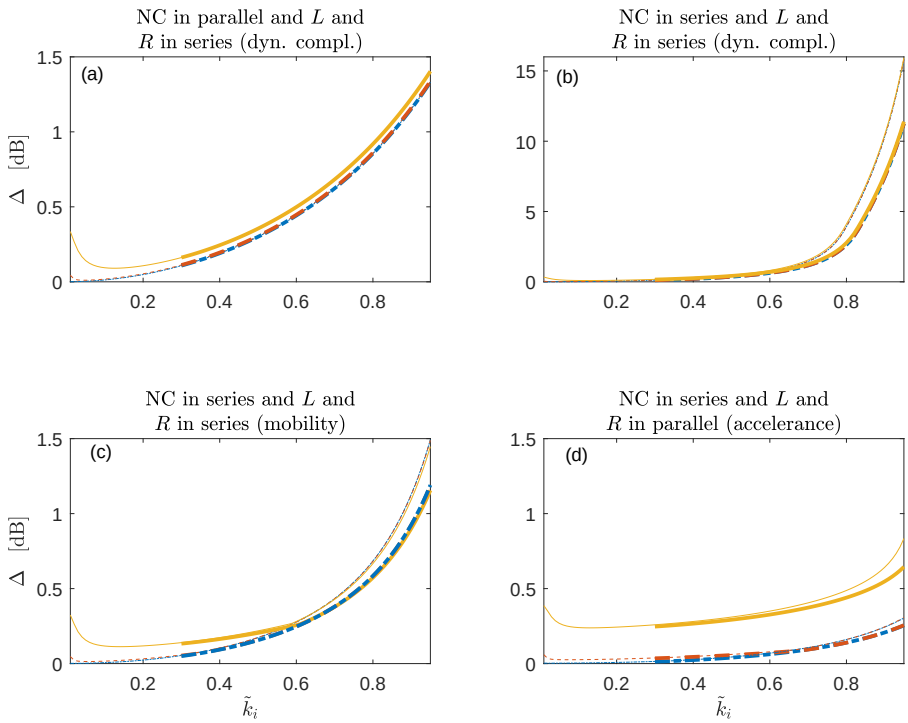

Figure 5. Δ for different systems with optimisation in terms of displacement (a and b), velocity (c) and acceleration (d). Thin lines for k_i=0.01 and thick lines for k_i=0.3; solid lines for $\xi_i = 10^{-2}$, dashed lines for $\xi_i = 10^{-3}$, dash-dotted lines for $\xi_i = 10^{-4}$.

This section analyses the attenuation performances achievable with the resonant shunt enhanced by NCs when the optimisation formulas of Tab. 4 are used. To this purpose, the attenuation is estimated using the A_{dB} index (expressed in decibel) defined as:

$$A_{\mathrm{dB}} = 20\log_{10}\frac{H_{\mathrm{sc}}}{H_{\mathrm{shunt}}} = 10\log_{10}\frac{H_{\mathrm{sc}}^2[(C|_{\Omega=\omega_{\mathrm{F}-}})^2 + (D|_{\Omega=\omega_{\mathrm{F}-}})^2]}{(A|_{\Omega=\omega_{\mathrm{F}-}})^2 + (B|_{\Omega=\omega_{\mathrm{F}-}})^2} \tag{7}$$

H_{sc} in Eq. (7) denotes the maximum value of $|H_i(\Omega)|$ in the SC condition without any NC. Its value is $1/(2\xi_i\omega_i^2\sqrt{1-\xi_i^2})$ in the case of dynamic compliance, $1/(2\xi_i\omega_i)$ for mobility and $1/(2\xi_i\sqrt{1-\xi_i^2})$ for accelerance. H_{shunt} is the amplitude of $H_i(\Omega)$ at $\omega_{\mathrm{F}-}$ (Thomas et al. (2012)) with the resonant shunt (coupled to NCs) tuned optimally. These two terms, H_{sc} and H_{shunt}, are expressed in displacement (over force) if the optimisation

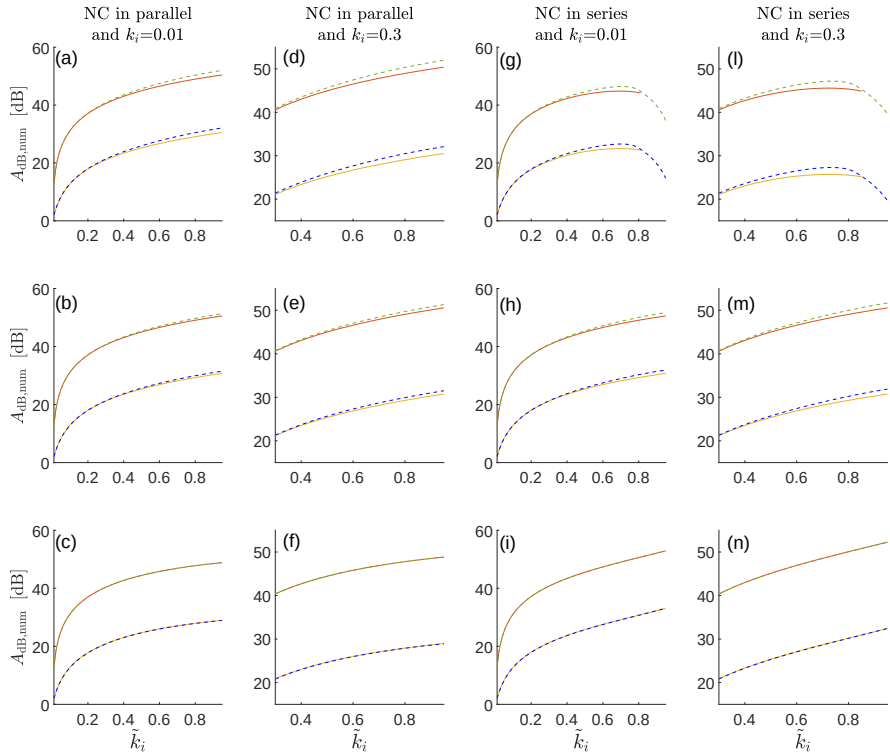

Figure 6. $A_{\mathrm{dB,num}}$ for different ξ_i values (10^{-2} for the curves in the lower part of each plot and 10^{-3} for the curves in the upper part of each plot): control in terms of displacement (a,d,g,l), control in terms of velocity (b,e,h,m), control in terms of acceleration (c,f,i,n). Solid lines for L and R connected in parallel and dashed lines for L and R connected in series.

is in terms of displacement, in terms of velocity (over force) if the optimisation is in terms of velocity, and in acceleration (over force) if the optimisation is in terms of acceleration. Thanks to the flat shape of the amplitude of the FRF in the optimally tuned condition (Fig. 2), $|H_i(\Omega)|$ at $\omega_{\mathrm{F}-}$ can be considered as a reliable approximation of the peak of $|H_i(\Omega)|$. A_{dB} can be shown to be always non-dependent on the value of ω_i.

It is possible to write A_{dB} for the different considered cases as a function of ξ_i, k_i and $\tilde{k}_i$ using the procedure reported in (Berardengo et al. (2016b)), where ω_i^{sc} and ω_i^{oc} are expressed as functions of k_i and $\tilde{k}_i$. In some cases, the expression is short and easy to write. As an example, in case of mobility and R and L connected in parallel, all the NC layouts lead to the same expression:

$$A_{\mathrm{dB}} = 10\log_{10}\frac{\tilde{k}_i^2 + 2\xi_i(4\xi_i + \sqrt{6\tilde{k}_i^2})}{8\xi_i^2} \tag{8}$$

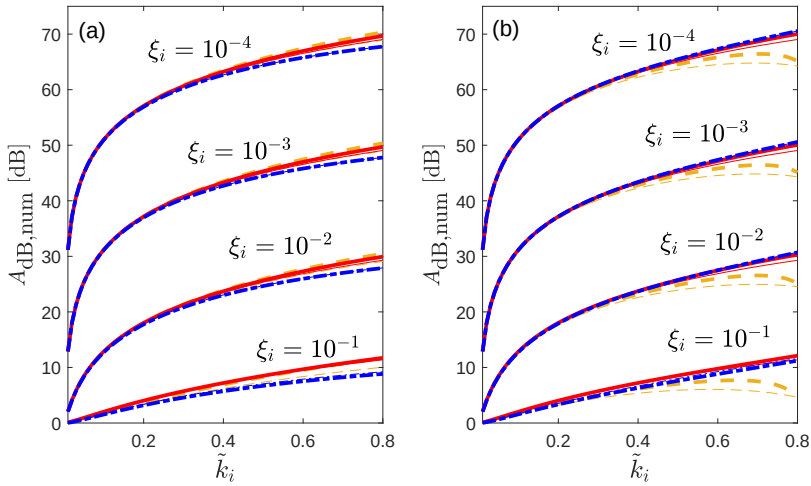

Figure 7. Trend of $A_{\mathrm{dB,num}}$ as a function of $\tilde{k}_i$ for different values of ξ_i and k_i=0.01 for an NC in parallel (a) and an NC in series (b). Thick lines for L and R connected in series and thin lines for L and R connected in parallel. Orange dashed lines for attenuation in terms of displacement, red solid lines for attenuation in terms of velocity, and blue dash-dotted lines for attenuation in terms of acceleration.

In this performance analysis, the case of the SP configuration for the NCs is not shown because it tends to a pure series NC configuration if C_1 tends to zero, and to a pure parallel NC configuration if C_2 tends to ∞ (Fig. 1b-d). This result has been already highlighted in (Berardengo et al. (2018)) for the case of the dynamic compliance, where the attenuation curves of the parallel were found to be slightly higher than those of the series and the SP curves resulted between them. The same result is thus expected and confirmed by the model in the case of mobility and accelerance. The only difference is that, in these two cases, the attenuation curve of the NC in series is slightly higher than that of the NC in parallel.

It is underlined that the index A_{dB} has been calculated considering the amplitude of the controlled FRF at ω_{F^-} (i.e. H_{shunt}). This is a reliable approximation when the structural damping is null (i.e. $\xi_i = 0$, see Berardengo et al. (2018)). However, in practical applications, $\xi_i \neq 0$, and in this case the $|H_i|$ curves no longer cross at points F^+ and F^-, although they remain close to this condition in case the ξ_i value is small enough. However, in order to verify if a non-null ξ_i value leads to attenuation values different from those expected using the A_{dB} formulation (due to the fact that the maximum of the FRF could be at a frequency value different from ω_{F^-}) for the different shunt configurations, also the actual attenuation calculated in decibels (i.e. related to the actual maximum of the FRF amplitude), named here $A_{\mathrm{dB,num}}$, has been computed numerically as:

$$A_{\mathrm{dB,num}} = 20\log_{10}\frac{H_{\mathrm{sc}}}{H_{\mathrm{num}}} \tag{9}$$

where H_{num} is the actual maximum of the amplitude of the controlled FRF when optimal values of ω_{e} and ξ_{e} are used (i.e. Tab. 4). Therefore, the difference between H_{num} (see Eq. (9)) and H_{shunt} (see Eq. (7)) is that H_{shunt} is the controlled FRF amplitude at ω_{F^-}, which is an approaximation of the actual FRF peak amplitude H_{num}.

The difference between A_{dB} and $A_{\mathrm{dB,num}}$ has been evaluated by defining the variable Δ:

$$\Delta = A_{\mathrm{dB}} - A_{\mathrm{dB,num}} \tag{10}$$

The trend of Δ as a function of $\tilde{k}_i$ for dynamic compliance, mobility and accelerance has been calculated for all the types of connection between L and R and type of connection of the NC and for some systems chosen as examples. These trends are reported in Figs. 5a and b for those configurations which show a value of Δ higher than 0.5 dB in a certain $\tilde{k}_i$ range in the case of the dynamic compliance. The two cases in which the value of Δ increases over 0.5 dB are for the NC in parallel and L and R connected in series (Fig. 5a), where however the maximum Δ value is acceptable, and for the NC in series (and also SP) and L and R connected in series (Fig. 5b). In this latter case, the value of Δ strongly increases for very high values of $\tilde{k}_i$ (i.e. over about 0.8, Fig. 5b). This occurs because, with this configuration, the amplitude of the controlled FRF at very low frequency (i.e. few Hertz) increases and becomes higher than at resonance.

Considering mobility and accelerance, A_{dB} is always an accurate estimation of $A_{\mathrm{dB,num}}$, being the values of Δ lower than 0.5 dB. The only cases in which this threshold is overcome are those related to Figs. 5c (for mobility) and d (for accelerance). However, in both the cases the highest values of Δ are always limited. Notice that, for some cases (especially accelerance), it is possible that for values of $\tilde{k}_i$ higher than those shown in the previous figures (i.e. higher than 0.95), together with high ξ_i values and low k_i values, A_{dB} could become not accurate in estimating $A_{\mathrm{dB,num}}$. However, these cases are of no practical interest because such high $\tilde{k}_i$ values are unlikely to be reached with low k_i values due to the instability limits and problems related to possible saturation of the operational amplifiers of the NCs.

Since NCs in series are effective for controlling modes at low frequency, while NCs in parallel are effective for controlling modes at high frequency (Berardengo et al. (2016b, 2018)), these two layouts are not compared here in terms of attenuation performance because they are usually used for different control problems, as mentioned. As for the SP, it can control modes in any frequency range (Berardengo et al. (2016b)) and, as mentioned, its performances are between those of the other two NC configurations.

An interesting comparison is instead that regarding the connection type between L and R. Figure 6 shows $A_{\mathrm{dB,num}}$ for both an NC in parallel and series for some systems chosen as examples. Plots (a,d,g,l) show that connecting L and R in series provides a higher attenuation performance at high $\tilde{k}_i$ values in terms of displacement. The attenuation

Table 5. Parameter values for the two systems used to simulate the case of high modal density ($\xi_i = 10^{-2}$ for all the modes of the table)

system 1			system 2		
mode number	$\omega_i/(2\pi)$ [Hz]	k_i	mode number	$\omega_i/(2\pi)$ [Hz]	k_i
1	500	0.15	1	100	0.15
2	1000	0.15	2	$\omega_3(1-\theta)$	0.15
3	$\omega_2(1+\theta)$	0.10	3	1000	0.15
4	1900	0.10	4	$\omega_3(1+\theta)$	0.10
–	–	–	5	1900	0.10

performances tend to become closer when considering velocity (see plots (b,e,h,m) and are almost equal in terms of acceleration (plots (c,f,i,n)).

The connection of L and R in series has shown to offer higher attenuations when controlling either displacement or velocity. Furthermore L and R connected in series allow to have lower values of L^{opt}, which in turn implies an easier practical implementation. However, another point deserves attention. Usually, L must be implemented employing operational amplifiers due to its high value (Moheimani and Fleming (2006)), and these circuits can generate additional parasitic resistances in series with the resulting inductances (Park and Inman (2003)). For the series connection of L and R, the compensation of these resistive parasitic effects can be straightforwardly carried out by changing R accordingly. Conversely, it is much more difficult to achieve this result when R and L are connected in parallel. Therefore, the series connection should be always preferred for an easier practical implementation of the entire circuit.

In order to have a quick comparison of the achievable attenuation levels, Fig. 7 shows the trend of $A_{\text{dB,num}}$ as a function of $\tilde{k}_i$ for different configurations of NC and connection between L and R, and also for different target variables (i.e. displacement, velocity, acceleration; each obtained using the corresponding optimisation criteria), for different values of ξ_i. Even if the plot is shown just for a system with k_i=0.01, these curves are also very close to the curves achievable for other values of k_i (actually, they are exactly the same when an NC in parallel is considered). Therefore, this figure can be considered as a sort of abacus, allowing to know in advance the maximum possible attenuation achievable when using the piezoeletric resonant shunt coupled to NCs.

Looking at Figs. 6 and 7, it can be also noticed that the attenuation levels achievable in terms of dynamic compliance, mobility and accelerance are close each other (given the same configuration of the NC) (compare, as an example, the curves of Figs. 6a, b, and c or look at the curves of Figs. 7a and b). When the value of $\tilde{k}_i$ becomes high, the attenuation curves of dynamic compliance, mobility and accelerance can differ of few decibels.

The case of high modal density

The optimisation formulas provided in this paper are valid in case of low modal density (see Section 'Model'). However, in Section 'Controlled FRFs', it has been mentioned

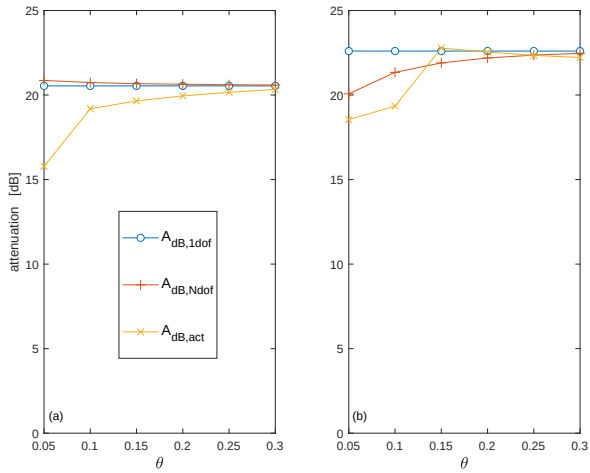

Figure 8. Trend of $A_{\mathrm{dB,1dof}}$, $A_{\mathrm{dB,Ndof}}$ and $A_{\mathrm{dB,act}}$ as a function of θ for the first (a) and the second (b) systems of Tab. 5. $\tilde{k}_2$=0.30 for system 1 and $\tilde{k}_3$=0.35 for system 2.

that, in case of high modal density, the optimisation formulas of Tab. 4 provide the starting values for seeking the actual optimal values of ω_{e} and ξ_{e}. Furthermore, even in presence of a significant modal superposition, in many cases the attenuation foreseen by the index A_{dB} using the optimal values coming from Tab. 4 is still able to provide a reliable estimation of the actual attenuation.

To show the above points, some examples are now discussed. To this purpose, a multi-degree-of-freedom system, chosen as an example, is simulated by means of the model presented in (Berardengo et al. (2017a)). In the first analysis, four modes are simulated and the aim is to attenuate the second one (at ω_2) in terms of acceleration; an NC in series is used. Table 5 (system 1) shows the values of ω_i, ξ_i and k_i for the four modes. Here, a parameter θ is used, and it expresses the relative distance between ω_3 and ω_2:

$$\theta = \frac{\omega_3 - \omega_2}{\omega_2} \tag{11}$$

Lower and lower values of θ mean that ω_3 becomes closer and closer to ω_2, making the modal superimposition higher and higher. Changing the value of θ, it is possible to increase/decrease the level of modal superimpostion of the two modes. It is also noticed that the chosen values of ξ_i are high for all the modes in order to increase the level of modal superimposition. Furthermore, also the eigenvector components are all set to 1 and the values of k_i are close. Indeed, both factors allow to make the influence of the other modes on the target mode high.

Three different indexes are then calculated: $A_{\mathrm{dB,1dof}}$, $A_{\mathrm{dB,Ndof}}$ and $A_{\mathrm{dB,act}}$. For all of them, the values of $\omega_{\mathrm{e}}^{\mathrm{opt}}$ and $\xi_{\mathrm{e}}^{\mathrm{opt}}$ have been set by means of the formulations proposed in Tab. 4. $A_{\mathrm{dB,1dof}}$ is the attenuation calculated by means of Eq. (7) and calculating ω_2^{sc} (which is affected by the presence of the NC) and ω_2^{oc} supposing to have negligible modal

superimposition and using the theoretical expressions provided in (Berardengo et al. (2016b)). Therefore, $A_{\mathrm{dB,1dof}}$ is the estimation of the attenuation in case of low modal density. $A_{\mathrm{dB,Ndof}}$ is the attenuation calculated again with Eq. (7) but in this case the values of ω_2^{sc} and ω_2^{oc} are directly estimated by carrying out a modal analysis of the FRF of the multi-degree-of-freedom system, which accounts for all the modes considered. In this way it is possible to take into account the modal contributions of the other modes. Indeed, when the modal superimposition is high, the actual values of ω_i^{sc} and ω_i^{oc} can become different from the theoretical expressions reported in (Berardengo et al. (2016b)). Finally, $A_{\mathrm{dB,act}}$ is the actual attenuation when all the modes are considered and again the values of ω_2^{sc} and ω_2^{oc} are found by means of a modal analysis of the FRF. Therefore, $A_{\mathrm{dB,Ndof}}$ can be seen as an approximation of $A_{\mathrm{dB,act}}$.

Figure 8a shows the trends of the three indexes as a function of the value of θ. The values of the indexes are close each other, exception made for $\theta = 0.05$, which is the case in which the modal superimposition becomes very high. Therefore, in all the other cases the expressions of Tab. 4 still constitute good approximations of the actual optimal values of ω_{e} and ξ_{e}.

Another example is provided in Fig. 8b. Here, five modes are simulated and the aim is to attenuate the third one (at ω_3) in terms of velocity using an NC in series. Table 5 (system 2) shows the values of ω_i, ξ_i and k_i for the five modes. In this case, the parameter θ expresses the relative distance between ω_3 and ω_2 and between ω_3 and ω_4:

$$\theta = \frac{\omega_3 - \omega_2}{\omega_3} = \frac{\omega_4 - \omega_3}{\omega_3} \tag{12}$$

The results of this example are close to those of the previous case. Therefore, the formulations proposed in the paper to find the values of $\omega_{\mathrm{e}}^{\mathrm{opt}}$, $\xi_{\mathrm{e}}^{\mathrm{opt}}$ and the attenuation can be used and guarantee good estimations of the optimal values of L, R and of the actual attenuation when the modal coupling is not very high; otherwise, they represent a good starting point from which the perfect tuning has to be looked for.

Experiments

The set-up employed was based on a cantilever beam with two piezoelectric patches bonded at the clamped end and electrically connected in series. This is the same set-up used in (Berardengo et al. (2018)), where more details can be found as well as all the procedures for estimating the system parameters.

The eigenfrequencies and non-dimensional damping ratios were estimated with experimental modal analysis with the piezoelectric actuator in SC (without NCs). The k_i values were found estimating ω_i^{sc} and ω_i^{oc} without NCs in the shunt circuit (see Eq. (3)). Since the different tests shown here were performed on different days, slight changes in the modal data occurred (see Section 'Results').

The inductance L was built using a synthetic circuit based on the Antoniou's circuit, where operational amplifiers are employed, because of its high values. The electrical layouts used for implementing the NC (together with the values of all the electric components of the circuit) can be found in Berardengo et al. (2018).

Results

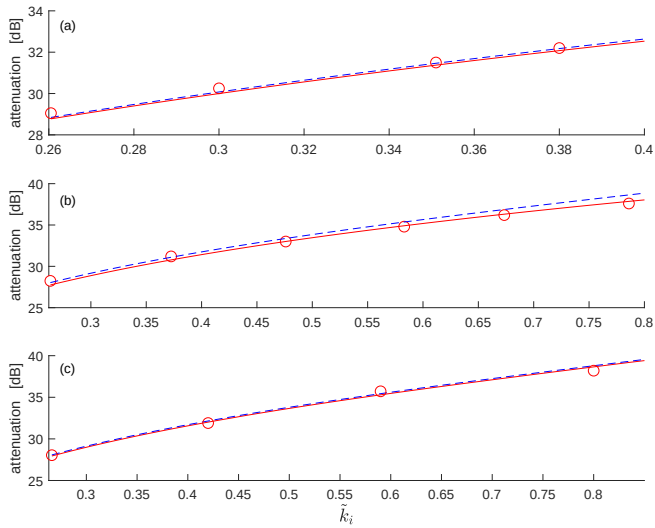

Figure 9. Theoretical expectations (dashed line for A_{dB} and solid line for $A_{\mathrm{dB,num}}$) and experimental results (circles) for Test A (a), Test B (b) and Test C (c).

The tests were carried out on the first mode of the beam aiming at validating the formulations derived for the values of $\omega_{\mathrm{e}}^{\mathrm{opt}}$ and $\xi_{\mathrm{e}}^{\mathrm{opt}}$ (Tab. (4)) for velocity and acceleration, as well as the corresponding A_{dB} values (Eq. (7)). For the displacement optimisation, the results have been already validated in Berardengo et al. (2018). In the experiments, the first mode (with an estimated value of C_{p1} of 39.38 nF) was chosen because of its high magnitude. All the tests shown here were performed with the series connection between L and R because of its advantages (see previously). As an example, Fig. 9 shows the attenuation curves for the following tests:

- optimisation in terms of mobility, NC in parallel, $\omega_1/(2\pi)$=34.45 Hz, ξ_1=0.35%, k_1=0.2605 (Test A);
- optimisation in terms of mobility, NC in series, $\omega_1/(2\pi)$=34.45 Hz, ξ_1=0.40%, k_1=0.2634 (Test B);
- optimisation in terms of accelerance, NC in series, $\omega_1/(2\pi)$=34.50 Hz, ξ_1=0.38%, k_1=0.2660 (Test C).

Furthermore, Figs. 10a and b show the comparison between experimental and numerical FRFs for one case of test C and one case of test B, respectively. The agreement between analytical and experimental results is good. Therefore, the analytical expressions derived in the paper for the optimisation of the shunt impedance can be considered as validated, as well as the formulas for the prediction of the attenuation.

Figures 10c and d show the experimental FRFs of Fig. 10b (that are in mobility with optimisation for mobility) in terms of displacement and acceleration, respectively.

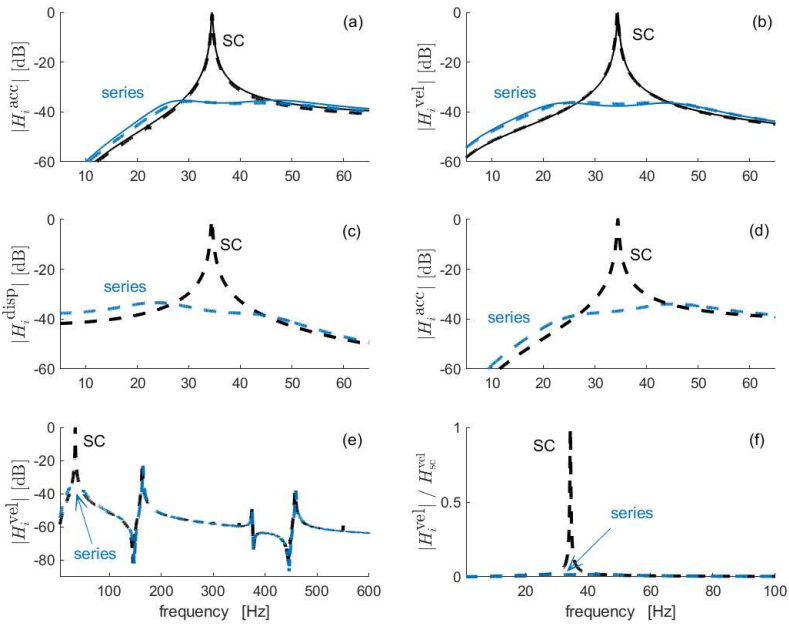

Figure 10. FRFs in terms of accelerance with an NC in series and $\tilde{k}_i$=0.5948 (Test C), L^{opt}=67.59 H, R^{opt}=13.04 kΩ (a), and FRFs in terms of mobility with an NC in series and $\tilde{k}_i$=0.6734 (Test B), L^{opt}=61.10 H, R^{opt}=12.21 kΩ (b). Experimental FRFs of plot b depicted in terms of dynamic compliance (c) and accelerance (d). Experimental FRFs of plot b on a wide frequency range (e), and in linear scale (f). Solid curves for the model expectations and dashed curves for the experiments.

Although a good attenuation effect can be noticed, it is evident that the controlled FRFs of plots (c) and (d) are not properly tuned because the optimisation is carried out in mobility. This is in agreement with the results shown in Fig. 2.

Finally, Fig. 10e shows the experimental FRFs of Fig. 10b on a wide frequency range in order to evidence that the shunt control works only on the targeted resonance (i.e. the first one in this case), and does not affect the trend of the FRF in other frequency ranges. Furthermore, Fig. 10f depicts the experimental FRFs of Fig. 10b with linear scale on the vertical axis (the FRFs are normalised, having the FRF in SC with unitary height, in order to allow for a straightforward percentage check) to stress the high attenuation provided by the shunt, that even leads to the cancellation of the resonance.

Guidelines

When NCs are employed, it is important to use the proper tuning criteria according to the type of variable to be minimised. Indeed, the values of L^{opt} and R^{opt} become farther farther for displacement, velocity and acceleration attenuation when the value of $\tilde{k}_i$ increases due to NCs.

Considering the connection type between L and R, the series offers higher attenuation levels than the parallel when controlling either displacement or velocity.

Regarding the NC type, it must be chosen according to the order of the mode to be damped: NCs in either SP or series are more advisable for low order modes, and either SP or parallel for high order modes.

Two further aspects are worthy of attention. One is related to the value of L^{opt}. Often, when controlling modes at low frequency, this value is high and thus implies problems related to the practical implementation. This paper evidences that the use of an NC in series, coupled to L and R connected in series, allows to achieve at the same time two different goals: an increase of the attenuation performance and a decrease of the value of L^{opt}, which in turn implies an easier practical implementation of the shunt circuit. The second important aspect is that when the value of $\tilde{k}_i$ increases due to NCs, the values of R^{opt} for the two connection types of L and R get closer and closer, making their levels of robustness to mistuning closer and closer.

Conclusion

This paper has addressed the optimisation of the piezoelectric resonant shunt enhanced by the use of NCs. The electric impedance connected to the piezoelectric actuator is made from a resistance, an inductance, and one or two NCs. The paper shows that it is possible to derive closed analytical formulations for optimising the resistance and inductance values, and for the prediction of the consequent vibration attenuation, when the target is to attenuate displacement, velocity or acceleration. These formulations are valid for all the possible NC layouts. When either velocity or acceleration are the control target, the impedance tuning leads to advantageous networks in terms of practical problems because of the lower values of the optimal inductance compared to the case of tuning in terms of displacement. Moreover, the formulations for the attenuation prediction in terms of velocity and acceleration are in general more accurate than in the case of displacement.

The two possible connection types of the resistance and the inductance have been compared, showing that the series offers higher attenuation than the parallel and an easier practical implementation. Furthermore, the paper suggests how to decrease the value of L^{opt}, increasing at the same time the attenuation performance.

Acknowledgment

This research has financially been supported at University of Parma by the Programme "FIL-Quota Incentivante" of University of Parma and co-sponsored by Fondazione Cariparma. Furthermore, the Italian Ministry of Education, University and Research is acknowledged by S. Manzoni (Politecnico di Milano) for the support provided through

the Project ”Department of Excellence LIS4.0 - Lightweight and Smart Structures for Industry 4.0”.

References

Andreaus U and Porfiri M (2007) Effect of electrical uncertainties on resonant piezoelectric shunting. *Journal of Intelligent Material Systems and Structures* 18: 477–485.

Beck BS, Cunefare KA and Collet M (2013) The power output and efficiency of a negative capacitance shunt for vibration control of a flexural system. *Smart Materials and Structures* 22(6). Article ID 065009.

Berardengo M, Manzoni S and Conti A (2017a) Multi-mode passive piezoelectric shunt damping by means of matrix inequalities. *Journal of Sound and Vibration* 405: 287–305.

Berardengo M, Manzoni S, Thomas O and Giraud-Audine C (2015) A new electrical circuit with negative capacitances to enhance resistive shunt damping. In: *Proceedings of the ASME 2015 Conference on Smart Materials, Adaptive Structures and Intelligent Systems - SMASIS 2015 - September 21-23, 2015 - Colorado Springs (CO, USA)*.

Berardengo M, Manzoni S, Thomas O and Vanali M (2018) Piezoelectric resonant shunt enhancement by negative capacitances: optimisation, performance and resonance cancellation. *Journal of Intelligent Material Systems and Structures* 29(12): 2581–2606.

Berardengo M, Manzoni S and Vanali M (2016a) The behaviour of mistuned piezoelectric shunt systems and its estimation. *Shock and Vibration* 2016. Article ID 9739217.

Berardengo M, Thomas O, Giraud-Audine C and Manzoni S (2016b) Improved resistive shunt by means of negative capacitance: new circuit, performances and multi mode control. *Smart Materials and Structures* 25. Article ID 075033.

Berardengo M, Thomas O, Giraud-Audine C and Manzoni S (2017b) Improved shunt damping with two negative capacitances: an efficient alternative to resonant shunt. *Journal of Intelligent Material Systems and Structures* 28(16): 2222–2238.

Bricault C, Pézerat C, Collet M, Pyskir A, Perrard P, Matten G and Romero-Garcia V (2019) Multimodal reduction of acoustic radiation of thin plates by using a single piezoelectric patch with a negative capacitance shunt. *Applied Acoustics* 145: 320–327.

Caruso G (2001) A critical analysis of electric shunt circuits employed in piezoelectric passive vibration damping. *Smart Materials and Structures* 10(5): 1059–1068.

Darleux R, Lossouarn B and Deü JF (2018) Passive self-tuning inductor for piezoelectric shunt damping considering temperature variations. *Journal of Sound and Vibration* 432: 105–118.

Date M, Kutani M and Sakai S (2000) Electrically controlled elasticity utilizing piezoelectric coupling. *Journal of Applied Physics* 87(2): 863–868.

de Marneffe B and Preumont A (2008) Vibration damping with negative capacitance shunts: theory and experiment. *Smart Materials And Structures* 17(3). Article ID 035015.

Ducarne J, Thomas O and Deü J (2012) Placement and dimension optimization of shunted piezoelectric patches for vibration reduction. *Journal of Sound and Vibration* 331(14): 3286–3303.

Fleming A, Behrens S and Moheimani S (2003) Reducing the inductance requirements of piezoelectric shunt damping systems. *Smart Materials and Structures* 12(1): 57–64.

Gardonio P and Casagrande D (2017) Shunted piezoelectric patch vibration absorber on two-dimensional thin structure: tuning considerations. *Journal of Sound and Vibration* 395: 26–47.

Gripp JAB and Rade DA (2018) Vibration and noise control using shunted piezoelectric transducers: A review. *Mechanical Systems and Siganl Processing* 112: 359–383.

Hagood N and von Flotow A (1991) Damping of structural vibrations with piezoelectric materials and passive electrical networks. *Journal of Sound and Vibration* 146: 243–268.

Høgsberg J and Krenk S (2015) Balanced calibration of resonant piezoelectric rl shunts with quasi-static background flexibility correction. *Journal of Sound and Vibration* 341: 16–30.

Høgsberg J and Krenk S (2017) Calibration of piezoelectric rl shunts with explicit residual mode correction. *Journal of Sound and Vibration* 386: 65–81.

Matveenko V, Iurlova N, Oshmarin D, Sevodina N and Iurlov M (2018) An approach to determination of shunt circuits parameters for damping vibrations. *International Journal of Smart and Nano Materials* 9(2): 135–149.

Moheimani S and Fleming A (2006) *Piezoelectric Transducers for Vibration Control and Damping*. Springer-Verlag.

Neubauer M, Oleskiewicz R, Popp K and Krzyzynski T (2006) Optimization of damping and absorbing performance of shunted piezo elements utilizing negative capacitance. *Journal of Sound and Vibration* 298(1-2): 84–107.

Park C and Inman D (2003) Enhanced piezoelectric shunt design. *Shock and Vibration* 10(2): 127–133.

Pohl M (2017) An adaptive negative capacitance circuit for enhanced performance and robustness of piezoelectric shunt damping. *Journal of Intelligent Material Systems and Structures* 28(19): 2633–2650.

Thomas O, De$\ddot{u}$ JF and Ducarne J (2009) Vibration of an elastic structure with shunted piezoelectric patches: efficient finite-element formulation and electromechanical coupling coefficients. *International Journal of Numerical Methods in Engineering* 80(2): 235–268.

Thomas O, Ducarne J and De$\ddot{u}$ J (2012) Performance of piezoelectric shunts for vibration reduction. *Smart Materials and Structures* 21(1). Article ID 015008.

Toftekær JF, Benjeddou A, Høgsberg J and Krenk S (2018) Optimal piezoelectric resistive-inductive shunt damping of plates with residual mode correction. *Journal of Intelligent Material Systems and Structures* 29(16): 3346–3370.

Yamada K, Matsuhisa H, Utsuno H and Sawada K (2010) Optimum tuning of series and parallel lr circuits for passive vibration suppression using piezoelectric elements. *Journal of Sound and Vibration* 329(24): 5036–5057.

Zhao G, Alujević N, Depraetere B and Sas P (2015) Dynamic analysis and h_2 optimisation of a piezo-based tuned vibration absorber. *Journal of Intelligent Material Systems and Structures* 26(15): 1995–2010.

Zhu Z, Lei W, Wang Q, Tiwari N and Hazra B (2020) Study on wind-induced vibration control of linked high-rise buildings by using tmdi. *Journal of Wind Engineering & Industrial Aerodynamics* 205. Article ID 104306.